

Direct Characterization of Kerogen by X-ray and Solid-State ^{13}C Nuclear Magnetic Resonance Methods

S. R. Kelemen,* M. Afeworki, M. L. Gorbaty, M. Sansone, P. J. Kwiatek, C. C. Walters, H. Freund, and M. Siskin

ExxonMobil Research and Engineering Co., Annandale, New Jersey 08801

A. E. Bence

ExxonMobil Upstream Research Co, Houston, Texas 77252

D. J. Curry

ExxonMobil Exploration Co., PO Box 2189, Houston, Texas 77060

M. Solum and R. J. Pugmire

Departments of Chemical Engineering and Chemistry, University of Utah, Salt Lake City, Utah 84112

M. Vandembroucke, M. Leblond, and F. Behar

IFP, Geology-Geochemistry Division, 92852 Rueil Malmaison, France

Received July 14, 2006. Revised Manuscript Received January 26, 2007

A combination of solid-state ^{13}C NMR, X-ray photoelectron spectroscopy (XPS) and sulfur X-ray absorption near edge structure (S-XANES) techniques are used to characterize organic oxygen, nitrogen, and sulfur species and carbon chemical/structural features in kerogens. The kerogens studied represent a wide range of organic matter types and maturities. A van Krevelen plot based on elemental H/C data and XPS derived O/C data shows the well established pattern for type I, type II, and type III kerogens. The anticipated relationship between the Rock–Eval hydrogen index and H/C is independent of organic matter type. Carbon structural and lattice parameters are derived from solid-state ^{13}C NMR analysis. As expected, the amount of aromatic carbon, measured by both ^{13}C NMR and XPS, increases with decreasing H/C. The correlation between aromatic carbon and Rock–Eval T_{max} , an indicator of maturity, is linear for types II and III kerogens, but each organic matter type follows a different relationship. The average aliphatic carbon chain length (C_n) decreases with an increasing amount of aromatic carbon in a similar manner across all organic matter types. The fraction of aromatic carbons with attachments (FAA) decreases, while the average number of aromatic carbons per cluster (C) increases with an increasing amount of aromatic carbon. FAA values range from 0.2 to 0.4, and C values range from 12 to 20 indicating that kerogens possess on average 2- to 5-ring aromatic carbon units that are highly substituted. There is basic agreement between XPS and ^{13}C NMR results for the amount and speciation of organic oxygen. XPS results show that the amount of carbon oxygen single bonded species increases and carbonyl–carboxyl species decrease with an increasing amount of aromatic carbon. Patterns for the relative abundances of nitrogen and sulfur species exist regardless of the large differences in the total amount of organic nitrogen and sulfur seen in the kerogens. XPS and S-XANES results indicate that the relative level of aromatic sulfur increases with an increasing amount of aromatic carbon for all kerogens. XPS show that the majority of nitrogen exists as pyrrolic forms in comparable relative abundances in all kerogens studied. The direct characterization results using X-ray and NMR methods for nitrogen, sulfur, oxygen, and carbon chemical structures provide a basis for developing both specific and general average chemical structural models for different organic matter type kerogens.

1. Introduction

Understanding the molecular structure and chemistry of complex organic sedimentary solids, such as kerogens, coals, and pyrobitumens, is aided by developing representative chemical structural models of these materials. In the past, significant advances were made using an indirect characterization approach

where the strategy employed was to decompose the solid thermally and then separate, identify, and quantify the evolved liquid and gaseous components. Incomplete decomposition of the organic solid and unknown chemical transformations that occur during pyrolytic decomposition are inherent limitations and impose associated uncertainties. Another approach was to employ selective/nondestructive chemical derivatizations or selective chemical cleavages, which also have intrinsic errors

* Corresponding author. Phone: (908) 730-2389.

due to incomplete or nonselective reactions and to inaccuracies of the quantification methods. The large amount of chemical data resulting from these types of characterization techniques must be integrated with other information, such as elemental composition, and synthesized to reconstruct molecular models of the organic solids. Representative models of the chemical structure of kerogen¹⁻³ and coal⁴⁻⁶ have been developed using these destructive approaches.

Significant advances in the late 1980s and 90s in direct solid-state measuring techniques (¹³C NMR, X-ray photoelectron spectroscopy (XPS), X-ray absorption near edge structure (XANES), Fourier transform infrared (FTIR), etc.) allowed hydrocarbon structures and organic nitrogen, sulfur, and oxygen forms to be speciated and quantified in complex organic materials. The advantage of direct characterization is that whole, unaltered, solid samples are analyzed, preserving structural information destroyed by decompositional methods. Recent models of coal have relied heavily on information obtained using direct characterization methods.⁷⁻¹² One drawback of solid-state analyses is that the information obtained must be viewed as an averaged composition. The development of representative models of complex, sedimentary organic solids is best served using results from both direct and indirect characterization approaches.

¹³C NMR is a powerful way to derive carbon chemical and structural parameters.¹³⁻¹⁵ Variable contact time and dipolar-dephasing NMR experiments, together with normal cross-polarization magic-angle spinning (CPMAS) integrations over selected chemical shift ranges, are used to derive parameters directly related to the carbon skeletal structure and lattice parameters.¹³ Both solid-state ¹³C NMR¹³⁻¹⁷ and XPS¹⁸ are capable of providing detailed information about the amount and form of aromatic carbons present in complex carbonaceous materials. Systematic ¹³C NMR investigations have been made

on coal,^{13,16} engine deposits,¹⁴ combustion soot,¹⁵ and crude oil asphaltenes.¹⁷

Information on the nature of organic oxygen functionalities in solids may be obtained using established wet chemical procedures^{19,20} or by infrared (IR) spectroscopy, which yields qualitative estimates of organic oxygen species.^{21,22} Solid-state ¹³C NMR analysis¹³⁻¹⁵ and XPS^{14,24} have proven capable of quantifying organic oxygen species in coals and other carbonaceous solids. The carbon signal from ¹³C NMR and carbon (1s) XPS are sensitive to chemical shifts caused by bonding to oxygen. The interpretation of ¹³C NMR and XPS data for the bound oxygen's effect on the carbon signal rely on different underlying assumptions and a comparison of results from ¹³C NMR and XPS has the potential to reveal different aspects of organic oxygen functional groups in kerogens. Advances in XPS^{25,26} and sulfur X-ray absorption near edge structure spectroscopy (S-XANES)²⁶⁻³⁶ methods offer a way to investigate directly organically bound and inorganic sulfur forms in complex carbonaceous materials such as kerogen. Likewise, recent advances in ¹⁵N NMR,^{26,37,38} XPS,^{26,39,40} and nitrogen X-ray absorption near edge structure (N-XANES) spectroscopy^{41,42} have provided new tools to probe the chemical structure of nitrogen forms in complex organic solids.

In this study, NMR and X-ray methods are used to characterize a suite of kerogens comprised of different organic matter types and levels of maturity. A combination of solid-state ¹³C NMR and XPS are used to quantify carbon chemical and structural features and organic oxygen species in kerogen. In the past, there has been considerable debate concerning the quantitative nature of ¹³C NMR for determining the percentage

(1) Siskin, M.; Scouten, C. G.; Rose, K. D.; Axzel, T.; Colgrove, S. G.; Pabst, R. E., Jr. Detailed Structural Characterization of the Organic Material in Rundle, Ramsey Crossing and Green River Oil Shales. In *Composition, Geochemistry and Conversion of Oil Shales*; Snape, C., Ed.; NATO ASI Series; Kluwer Academic Publishers: London, 1995.

(2) Behar, F.; Vandenbroucke, M. *Rev. Inst. Franc. Pet. (Oil Gas Sci. Technol.)* **1986**, *41*, 173-188.

(3) Behar, F.; Vandenbroucke, M. *Org. Geochem.* **1987**, *11*, 15-24.

(4) Solomon, P. R. Coal structure and thermal decomposition. In *New Approaches in Coal Chemistry*; Blaustein, B. D.; Bockrath, B. C.; Friedman, S., Eds.; ACS Symposium Series 169; American Chemical Society: Washington, DC, 1981; pp 61-71.

(5) Shinn, J. H. *Fuel* **1984**, *63*, 1187.

(6) Given, P. H. *Fuel* **1960**, *39*, 147.

(7) Faulon, J. L.; Vandenbroucke, M.; Drappier, J. M.; Behar, F.; Romero, M. *Org. Geochem.* **1990**, *16*, 981.

(8) Carlson, G. A. *Energy Fuels* **1992**, *6*, 771.

(9) Fletcher, T. H.; Kerstein, A. K.; Pugmire, R. J.; Solum, M. S.; Grant, D. M. *Energy Fuels* **1992**, *6*, 414.

(10) Faulon, J. L.; Carlson, G. A.; Hatcher, P. G. *Energy Fuels* **1993**, *7*, 1062.

(11) Takanohashi, T.; Kawashima, H. *Energy Fuels* **2002**, *16*, 379.

(12) Mathews, J. P.; Hatcher, P. G.; Scaroni, A. W. *Energy Fuels* **2001**, *15*, 863.

(13) Solum, M. S.; Pugmire, R. J.; Grant, D. M. *Energy Fuels* **1989**, *3*, 187.

(14) Kelemen, S. R.; Siskin, M.; Homan, H. S.; Pugmire, R. J.; Solum, M. S. *SAE Tech. Pap. Ser.* **1998**, no. 982715.

(15) Solum, M. S.; Sarofim, A. F.; Pugmire, R. J.; Fletcher, T. H.; Zhang, H. *Energy Fuels* **2001**, *15*, 961.

(16) Snape, C. E.; Axelson, D. E.; Botto, R. E.; Delpuech, J. J.; Tekely, P.; Gerstein, B. C.; Pruski, M.; Maciel, G. E.; Wilson, M. A. *Fuel* **1989**, *68*, 547.

(17) Calemma, P.; Iwanski, P.; Nali, M.; Scotti, R.; Montanari, L. *Energy Fuels* **1995**, *9*, 225.

(18) Kelemen, S. R.; Rose, K. D.; Kwiatek, P. J. *Appl. Surf. Sci.* **1993**, *64*, 167.

(19) Blom, L.; Edelhause, L.; van Krevelen, D. W. *Fuel* **1957**, *36*, 135.

(20) Marata, S.; Hosokawa, M.; Kidena, K.; Nomura, M. *Fuel Process. Technol.* **2000**, *67*, 231.

(21) Kuehn, D. W.; Snyder, R. W.; Davis, A.; Painter, P. C. *Fuel* **1982**, *61*, 682.

(22) Dyrkacz, G. R.; Bloomquist, C. A.; Solomon, P. R. *Fuel* **1984**, *63*, 536.

(23) Kelemen, S. R.; Afeworki, M.; Gorbaty, M. L.; Cohen, A. D. *Energy Fuels* **2002**, *16*, 1450.

(24) Kelemen, S. R.; Kwiatek, P. J. *Energy Fuels* **1995**, *9*, 841.

(25) Kelemen, S. R.; George, G. N.; Gorbaty, M. L. *Fuel* **1990**, *69*, 939.

(26) Kelemen, S. R.; Afeworki, M.; Gorbaty, M. L.; Kwiatek, P. J.; Sansone, M.; Walters, C. C.; Cohen, A. D. *Energy Fuels* **2006**, *20*, 635.

(27) Gorbaty, M. L.; George, G. N.; Kelemen, S. R. *Fuel* **1990**, *69*, 945.

(28) Huffman, G. P.; Mitra, S.; Huggins, F. E.; Shah, N.; Vaidya, F.; Lu, F. *Energy Fuels* **1991**, *5*, 574.

(29) George, G. N.; Gorbaty, M. L.; Kelemen, S. R.; Sansone, M. *Energy Fuels* **1991**, *5*, 93.

(30) Wilfong, R.; Mitra-Kirtley, S.; Mullins, O. C.; Andrews, B.; Fujisawa, G.; Larsen, J. W. *Energy Fuels* **2005**, *19*, 1971.

(31) Mitra-Kirtley, S.; Mullins, O. C.; van Elp, J.; George, S. J.; Chen, J.; Cramer, S. P. *J. Am. Chem. Soc.* **1993**, *115*, 252.

(32) Riboulleau, A.; Derenne, S.; Saret, G.; Largeau, C.; Baudin, F.; Connan, J. *Org. Geochem.* **2000**, *31*, 1641.

(33) Saret, G.; Mongenot, T.; Connan, J.; Derenne, S.; Kasrai, M.; Bancroft, G. M.; Largeau, C. *Org. Geochem.* **2002**, *33*, 877.

(34) Saret, G.; Connan, J.; Kasrai, M.; Bancroft, G. M.; Charrie-Duhaut, A.; Lemoine, S.; Adam, P.; Albrecht, P.; Eybert-Berard, L. *Geochim. Cosmochim. Acta* **1999**, *63*, 3767.

(35) Kasrai, M.; Bancroft, G. M.; Brunner, R. W.; Jonasson, R. G.; Brown, J. R.; Tan, K. H.; Feng, X. *Geochim. Cosmochim. Acta* **1994**, *58*, 2865.

(36) Eglinton, T. I.; Irvine, J. E.; Vairavamurthy, A.; Zhou, W.; Manowitz, B. *Org. Geochem.* **1994**, *22*, 781.

(37) Knicker, H. *Mar. Chem.* **2004**, *92*, 167.

(38) Kelemen, S. R.; Afeworki, M.; Gorbaty, M. L.; Kwiatek, P. J.; Solum, M. S.; Hu, J. Z.; Pugmire, R. J. *Energy Fuels* **2002**, *16*, 1507.

(39) Kelemen, S. R.; Freund, H.; Gorbaty, M. L.; Kwiatek, P. J. *Energy Fuels* **1999**, *13*, 529.

(40) Kelemen, S. R.; Gorbaty, M. L.; Kwiatek, P. J. *Energy Fuels* **1994**, *8*, 897.

(41) Mitra-Kirtley, S.; Mullins, O. C.; Branthaver, J. F.; Cramer, S. P. *Energy Fuels* **1993**, *7*, 1128.

(42) Vairavamurthy, A.; Wang, S. *Environ. Sci. Technol.* **2002**, *36*, 3050.

Table 1. Kerogen Rock–Eval Data and Hydrogen Content (per 100 Carbon) from Elemental Analysis

sample	kerogen type	elemental analysis hydrogen per 100 C	Rock-Eval	
			Tmax (°C)	hydrogen index (mg/g)
Green River	I	153	446	739
Rundle	I	164	444	995
Duvernay (A)	II	117	414	532
Duvernay (B)	II	111	438	439
Duvernay (C)	II	89	443	242
Duvernay (D)	II	56	479	22
Oxford Clay	II	123	413	577
Paradox	II	104	438	401
Malm	II	129	420	670
Draupne	II	108	424	581
Bakken	II	122	419	580
Monterey	IIS	135	411	621
Gippsland (A)	IIIC	88	415	251
Gippsland (B)	IIIC	80	436	226
Proprietary (A)	IIIC	87	427	295
Proprietary (B)	IIIC	76	453	235
Proprietary (C)	IIIC	61	479	120
Fruitiand	IIIC	89	424	237

↓ = thermal maturity sequence A= immature B-C = oil window, D = post-mature

of aromatic carbon in coal.¹⁶ Use of both ¹³C NMR and XPS serves as a self-consistent check since the techniques have different underlying assumptions and associated uncertainties for determining aromatic carbon. XPS is used to speciate and quantify nitrogen forms. A combination of S-XANES and XPS are used to speciate and quantify sulfur forms. The resulting chemical characterization of the suite of kerogens then may be used for development of representative specific chemical structure models.^{43,44}

2. Experimental and Results

2.1. Samples. A suite of kerogens was assembled that represent several major petroleum source facies. Lacustrine source rocks from the Green River and Rundle formations contain hydrogen-rich algal kerogen (type I) derived primarily from cyanobacteria or various Chlorophyta and dinoflagellates, respectively. Various marine environments are represented mostly by clastic source rocks containing kerogen (type II) derived primarily from marine planktonic organisms with small amounts of terrigenous plant debris. One sample from the Monterey Formation is a siliceous source rock containing kerogen that is comparatively enriched in organic sulfur (type IIS).

Hydrogen-rich kerogens derived primarily from higher plant remains are represented by type III kerogen in several coals and coaly shales. This type of organic matter, chemically distinct from that found in gas-prone vitrinitic coals, contains a variety of aliphatic-rich macerals (sporinite and liptinite, including alginite, cutinite, and suberinite) and is the source of major accumulations of paraffinic oil found principally in southeast Asia and west Africa.⁴⁵ We have designated such kerogens as type IIIC.⁴⁶ Two type IIIC samples from the Gippsland Basin differ slightly in maturity but, more importantly, in depositional setting. Sample A was deposited in a transitional coastal environment and incorporated sulfur during early diagenesis, while sample B has little or no marine influence.

There are two subsets of related kerogens within the suite of samples that represent equivalent source rocks at different levels of thermal maturity. Four type II samples are from the Duvernay

(43) Freund, H.; Walters, C. C.; Kelemen, S. R.; Siskin, M.; Gorbaty, M. L.; Curry, D. J.; Bence, A. E. *Org. Geochem.* **2007**, *38*, 288–305; <http://dx.doi.org/10.1016/j.orggeochem.2006.09.009>.

(44) Walters, C. C.; Freund, H.; Kelemen, S. R.; Peczak, P.; Curry, D. J. *Org. Geochem.* **2007**, *38*, 306–322; <http://dx.doi.org/10.1016/j.orggeochem.2006.09.010>.

(45) Wilkins, R. W. T.; George, S. C. *Int. J. Coal Geol.* **2002**, *50*, 317.

(46) Curry, D. J.; Emmett, J. K.; Hunt, J. W. *Geol. Soc. Spec. Publ.* **1994**, *77*, 149.

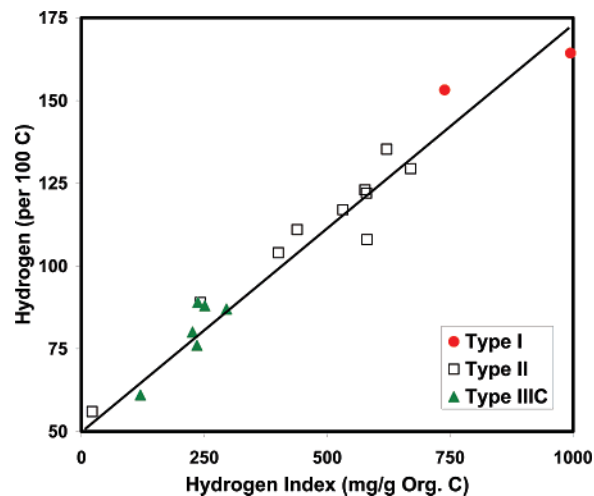


Figure 1. Comparison of Rock–Eval hydrogen index (HI) with elemental hydrogen per 100 carbons.

Formation and span the range from immature to postmature (~0–95% conversion). Three type IIIC samples are from an Asian location that is proprietary. These samples span the oil window (~10–60% conversion). The remaining samples are immature with respect to oil generation.

Types I and II kerogens were isolated from the rock matrix by mineral dissolution with HCl/HF according to the standard procedure described by Durand and Nicaise.⁴⁷ It is recognized that this procedure does not remove pyrite and other minerals protected by encapsulation by organic matter. Removal of pyrite was done only for ¹³C NMR analysis of Monterey type IIS by pretreatment with CrCl₂.⁴⁸ Kerogen type IIIC samples were not demineralized.

Rock–Eval data for the kerogens of this study are shown in Table 1 along with the amount of hydrogen expressed relative to carbon on a 100 carbon atom basis as measured by elemental analysis. These kerogens show the expected relationship between the Rock–Eval hydrogen index (HI) and hydrogen content that is independent of organic matter type⁴⁹ (Figure 1).

2.2. X-ray Photoelectron Spectroscopy (XPS). Freshly powdered samples were mounted on a metallic nub via nonconducting double-sided tape and analyzed by a Kratos Axis Ultra system using monochromatic Al K α radiation. The unit is equipped with automatic sample charge neutralization to ensure a uniform sample space charge. An energy correction was made to account for sample charging based on the carbon (1s) peak at 284.8 eV. The elemental concentrations are reported relative to carbon, calculated from XPS spectra based on the area of the characteristic photoelectron peaks after correcting for atomic sensitivity. The relative amount of aromatic carbon was determined by the method of Π to Π^* signal intensity.¹⁸ The amount of organic oxygen was derived from the total oxygen (1s) signal by taking into account inorganic contributions.²⁴ Table 2 lists the amount of aromatic carbon and organic oxygen in the kerogens on an atoms per 100 carbon basis as determined by XPS analysis.

Organic oxygen forms were determined by analyzing oxygen's effect on the XPS carbon (1s) signal of adjacent carbon atoms. Four peaks at 284.8, 286.3, 287.5, and 289.0 (± 0.1) eV are used to curve-resolve the XPS carbon (1s) signal. The 284.8 eV peak represents contributions from both aromatic and aliphatic carbon. The 286.3 eV peak represents carbon bound to one oxygen by a single bond (e.g., C–O, C–OH, etc.). The 287.5 eV peak corresponds to carbon bound to oxygen by two oxygen bonds (C=O). The 289.0 eV peak corresponds mainly to carbon bound to

(47) Durand, B.; Nicaise, G. In *Kerogen*; Durand, B., Ed. Editions Technip: Paris, 1980; pp 35–53.

(48) Acholla, F.; Orr, W. L. *Energy Fuels* **1993**, *7*, 406.

(49) Tissot, B. P. Welte. *Petroleum Formation and Occurrence*, 2nd ed.; Springer-Verlag: Berlin, 1984.

Table 2. Amount of Aromatic Carbon and Organic Oxygen from XPS

sample	amount (per 100 carbon)	
	aromatic carbon	organic oxygen
Green River	29	5.1
Rundle	19	11.1
Duverney (A)	40	9.7
Duverney (B)	43	5.9
Duverney (C)	54	5.0
Duverney (D)	72	4.7
Oxford Clay	32	13.7
Paradox	45	3.9
Malm	30	10.0
Draupne	47	4.1
Bakken	45	8.6
Monterey	33	14.9
Gippsland (A)	56	15.4
Gippsland (B)	63	10.6
Proprietary (A)	52	11.1
Proprietary (B)	71	6.6
Proprietary (C)	81	4.0
Fruitland	63	9.3

↓ = thermal maturity sequence A= immature B-C = oil window, D = post-mature

oxygen by three bonds (O=C—O). The relative full width at half-maximum (fwhm) values of all peaks in the ensemble were fixed, and all carbon (1s) spectra could be curve-resolved using fwhm = 1.5 (±0.1) eV.

Example XPS carbon (1s) spectra for kerogens and their curve-resolution into different organic oxygen components are shown in Figure 2. Results of analyses of the amount of organic oxygen associated with each carbon (1s) peak are listed in Table 3. One oxygen (e.g., C=O) is assumed to be associated with the 287.5 eV carbon (1s) peak, and two oxygens (e.g., O=C—O) are assumed to be associated with the 289.0 eV carbon (1s) peak. The amount of oxygen associated with the 286.3 eV carbon (1s) peak is determined from the difference between the total amount of organic oxygen and the amount of oxygen associated with the 287.5 and 289.0 eV carbon (1s) peaks.

Nitrogen forms in kerogen were defined and quantified using XPS. A detailed description of XPS curve-resolution methods for nitrogen appears elsewhere.^{38,40} Briefly, nitrogen (1s) kerogen spectra were curve-resolved using four peaks at fixed energy positions of 398.6, 399.4, 400.2, and 401.4 (±0.1) eV and fwhm = 1.4 (±0.1) eV. Figure 3 is illustrative of XPS nitrogen (1s) spectra and the curve-resolution into different components for several different kerogens. Solid-state ¹⁵N NMR of Green River Formation kerogen yields a dominant peak centered near -245 ppm, consistent with the position expected for pyrrolic nitrogen.^{38,50} On the basis of this evidence, the 400.2 eV peak in the Green River XPS spectra is attributed to pyrrolic nitrogen. Similarly, the 400.2 eV peak found in other types I and II kerogens is assigned to pyrrolic nitrogen forms. The unambiguous 398.6 eV pyridinic and the 401.4 eV quaternary nitrogen peaks are present in all kerogens. Quaternary nitrogen forms in types I and II kerogens are associated with protonated pyridinic or other basic nitrogen species including organic and inorganic forms and either are initially present and survived demineralization or are created during demineralization. Type IIIC kerogens were not demineralized, and in these cases, the quaternary nitrogen is associated clearly with naturally occurring protonated basic nitrogen species. Another peak at 399.4 eV, the position expected for amine forms of nitrogen, is needed to fully curve-resolve some kerogens where it may contribute ≥5 mol %. The quantitative results of XPS nitrogen (1s) curve-resolution for kerogen included in this study are shown in Table 4 on a mole percent basis as well the total the amount of nitrogen on a 100 carbon atom basis.

Sulfur speciation also was measured by XPS. The XPS sulfur (2p) spectrum from an individual component species is comprised of 2p_{3/2} and 2p_{1/2} components at a 2-to-1 intensity separated in energy by 1.2 eV. The XPS sulfur (2p) spectra for kerogens are

complex and are usually comprised of a low binding energy (~164 eV) signal and a higher binding energy (~168 eV) signal (see Figure 4). These signals were simultaneously curve-resolved using components with fixed energy positions and the full width at half-maximum (fwhm) values. The lower binding energy signal contains contributions from FeS₂ (162.5 ± 0.1 eV), aliphatic sulfur (163.3 ± 0.2 eV), aromatic sulfur (164.1 ± 0.1 eV), and sulfoxide (165.7 ± 0.3 eV) components having 2p_{3/2} and 2p_{1/2} components each with fwhm values 1.1 ± 0.1 eV. The higher energy signal was curve-resolved using two components at 168.0 ± 0.5 and 168.5 ± 0.5 eV having 2p_{3/2} and 2p_{1/2} components of fwhm 1.5 ± 0.5 eV. These signals overlap but are expected to arise predominantly from sulfate, but contributions from sulfite and sulfones cannot be entirely dismissed. Therefore, only the sum of the curve-resolved intensity for the 168.0 and 168.5 components is reported and is assigned collectively to sulfate, sulfite, and sulfone.

Example XPS sulfur spectra and their curve-resolution into different components are shown in Figure 4 and results for all kerogens are listed in Table 5. Inorganic sulfate and pyrite appear in nearly all spectra in addition to organic sulfur forms. Surface oxidation of pyrite is very rapid and unavoidable in even carefully handled samples⁵¹ and may be the source of the observed surface sulfate.

2.3. Solid-State ¹³C NMR. Solid-state ¹³C NMR spectra were recorded on the kerogens using two different spectrometers: one at ExxonMobil and the other at the University of Utah. The ExxonMobil spectrometer is a Chemagnetics CMXII-200 spectrometer operating at a static magnetic field of 4.7 T (50.2 MHz ¹³C). The samples were packed into a 5-mm diameter zirconia rotor and spun at 8 kHz. The kerogens were characterized by cross-polarization magic-angle spinning (CPMAS)/NMR experiments performed at a ¹H-¹³C CP contact time, typically 3 ms, and a pulse repetition delay of 2 s. The ¹H and ¹³C radio frequency fields were at 71.4 kHz for Hartmann-Hahn match during cross-polarization and the proton high power decoupling during data acquisition. The dipolar dephasing^{52,53} experiments were performed with a rotor-synchronized echo.⁵⁴ After the CP, the high power ¹H decoupling was turned off to dephase protonated carbons, typically for a period of 60–90 μs, and was turned back on for the rest of the two-rotor period and during ¹³C signal acquisition. A 180° pulse was applied on the ¹³C channel in the middle of the first rotor period for refocusing purposes. The full echo spectrum was recorded without interruption in the decoupling. High-resolution solid-state ¹³C NMR measurements of kerogen were performed at the University of Utah spectrometer using a Chemagnetics CMX-100 spectrometer with a 7.5 mm PENCIL rotor probe and a ¹³C NMR frequency of 25.152 MHz. All spectra were run with a 1-s pulse delay and 62.5 kHz of decoupling power. A 2-ms contact time was used on the dipolar dephased spectra, and on the 10 000 scan spectrum from which the subintegrals were taken. Data were obtained in an interleaved fashion for both the dipolar dephasing and variable contact time experiments with about 100 scans per tau value and about 30 whole cycles for about 3000 total scans for each tau value. The variable contact time experiments used 21 contact times ranging from 5 μs to 25 ms. The dipolar dephasing experiments used 23 interruption intervals from 2 to 200 μs. The levels of aromatic carbon and oxygen containing functional groups were determined from the CPMAS data using methods previously described.^{13–15} By a combination of a dipolar dephasing experiment (which allows the separation of protonated and nonprotonated aromatic carbons) with integrals from selected chemical shift ranges representing oxygen and carbon substituted aromatic carbons, the amount of bridgehead carbons may be quantified. This allows the determination of the average aromatic carbon ring size and average number of attachments to aromatic cores.¹³ The definition of ¹³C NMR structural

(51) Kelemen, S. R.; Gorbaty, M. L.; George, G. N.; Kwiatek, P. J. *Energy Fuels* **1991**, *5*, 720.

(52) Opella, S. J.; Frey, M. H. *J. Am. Chem. Soc.* **1979**, *101*, 5854.

(53) Alemany, L. B.; Grand, D. M.; Alger, T. D.; Pugmire, R. J. *Am. Chem. Soc.* **1983**, *105*, 6697.

(54) Newman, R. H. *J. Magn. Reson.* **1990**, *86*, 176.

(50) Knicker, H.; Scaroni, A. W.; Hatcher, P. G. *Org. Geochem.* **1996**, *24*, 661.

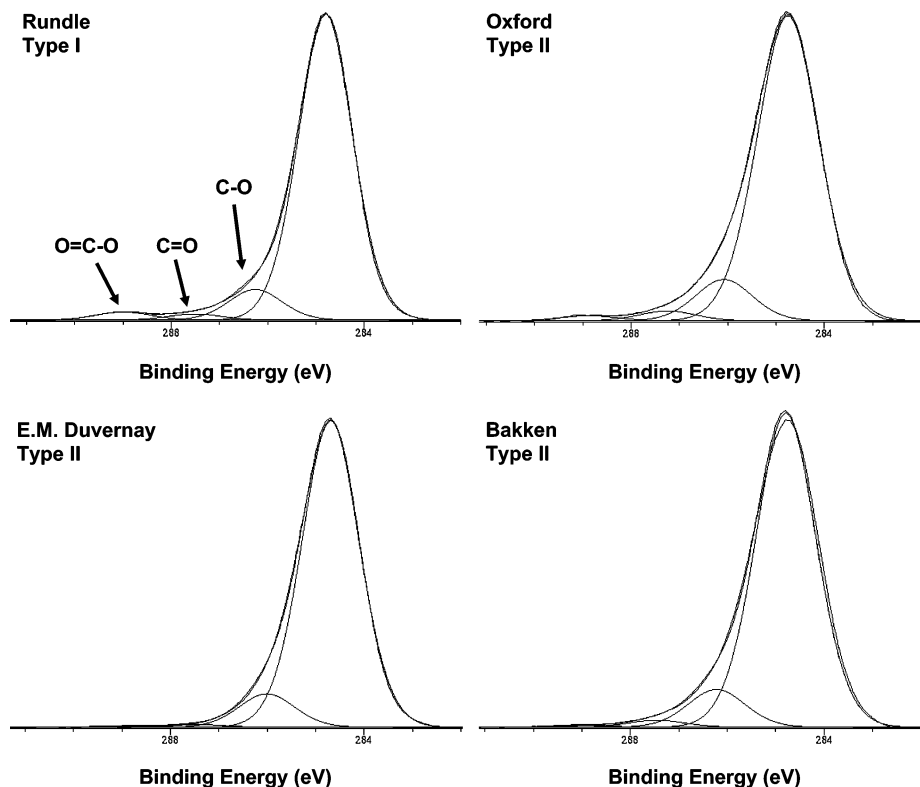


Figure 2. Example XPS carbon (1s) spectra for kerogen and curve-resolution into different components.

Table 3. XPS Results for Forms of Organic Oxygen

sample	amount (per 100 carbon)		
	C-O (286.3 eV) by difference	C=O (287.5 eV)	O-C=O 2x (289.0 eV)
Green River	3.8	0.5	0.8
Rundle	4.6	1.7	4.7
Duvernay (A)	5.0	3.4	1.3
Duvernay (B)	4.2	0.8	0.8
Duvernay (C)	3.5	0.8	0.7
Duvernay (D)	4.7	0.0	0.0
Oxford Clay	8.7	2.4	2.6
Paradox	2.2	0.6	1.1
Malm	6.8	2.8	0.4
Draupne	3.3	0.6	0.3
Bakken	6.5	1.8	0.3
Monterey	10.1	2.0	2.8
Gippsland (A)	9.5	2.8	3.1
Gippsland (B)	8.3	1.6	0.7
Proprietary (A)	6.8	2.2	2.1
Proprietary (B)	6.6	0.0	0.0
Proprietary (C)	4.0	0.0	0.0
Fruitland	7.1	1.9	0.3

↓ = thermal maturity sequence A= immature B-C = oil window, D = post-mature

parameters and chemical shift ranges are the same as those reported previously^{13–15} and are shown in Table 6.

Solid-state ¹³C NMR spectra obtained at the University of Utah for types I, II, and IIIC kerogens are shown in Figure 5. Solid-state ¹³C NMR spectra obtained at ExxonMobil for types II and IIIC kerogens are shown in Figures 6 and 7, respectively. All NMR spectra were self-consistently analyzed to obtain the chemical structural parameters listed in Table 7. NMR lattice parameters for the kerogens are listed in Table 8.

2.4. Sulfur X-ray Absorption Near Edge Structure (S-XANES). The sulfur XANES spectra were obtained at beam lines 6-2 at the Stanford Synchrotron Radiation Laboratory (SSRL) and the Advanced Photon Source at Argonne National Laboratory using techniques and protocols developed previously for speciation and quantification of organically bound sulfur forms in coals.^{27,29} The S-XANES analysis approach starts by obtaining a sulfur X-ray absorbance spectrum of the sample (Figure 8), taking the third

derivative of that spectrum (Figure 9), and curve-resolving the third derivative spectrum with a nonlinear least-squares regression program using the spectra and the third derivative spectra of model compounds. This method has been documented in detail.^{27,29} Each spectrum was curve fit using seven model components: pyrite, aliphatic sulfide, thiophenic sulfur, sulfoxide, sulfone, sulfite and sulfate. This is illustrated in Figure 10 for Duvernay (A) kerogen.

Results of the analyses of S-XANES of kerogens are listed in Table 9. The values are expressed as mole percent of total sulfur in the sample. Independent curve fits to the near edge absorbance spectra of each kerogen were made using the same model compounds identified in the analysis of the third derivative absorbance spectra. This curve fit is illustrated for the near edge spectrum from the Duvernay (A) kerogen in Figure 10, and the results for all kerogens are listed in Table 10. The agreement of these curve-resolutions is well within the experimental error of the method.

Aliphatic and aromatic organic sulfur forms are found in all kerogens. Oxidized sulfur forms include sulfoxide, sulfone, sulfite, and sulfate. In all cases the amount of sulfoxide and sulfone is low and only their sum is reported. In addition to organic forms of sulfur, pyrite and sulfate appear in nearly all kerogens. The lowest energy feature is due to the presence of pyrite while the highest energy feature is due to the presence of sulfate. A close correspondence between XPS and S-XANES analyses for pyrite and sulfate is not expected as the amount of iron at the surface can be very different than the bulk average due to a number of factors that include encapsulation of pyrite by organic matter and particle size effects.⁵¹

The presence of significant quantities pyrite adds complexity in fitting the third derivative S-XANES spectrum and deciphering the nonoxidized organic sulfur forms. In the absence of pyrite, a distinction among aliphatic sulfur forms (i.e., sulfide and disulfide)²⁶ and among aromatic sulfur forms (i.e., aryl sulfide and thiophenic)²⁷ can be made. In general, including aliphatic disulfide and aryl sulfide model compound spectra in the curve fitting process of kerogen together with aliphatic sulfide and thiophenic model compound spectra did not significantly improve or diminish the

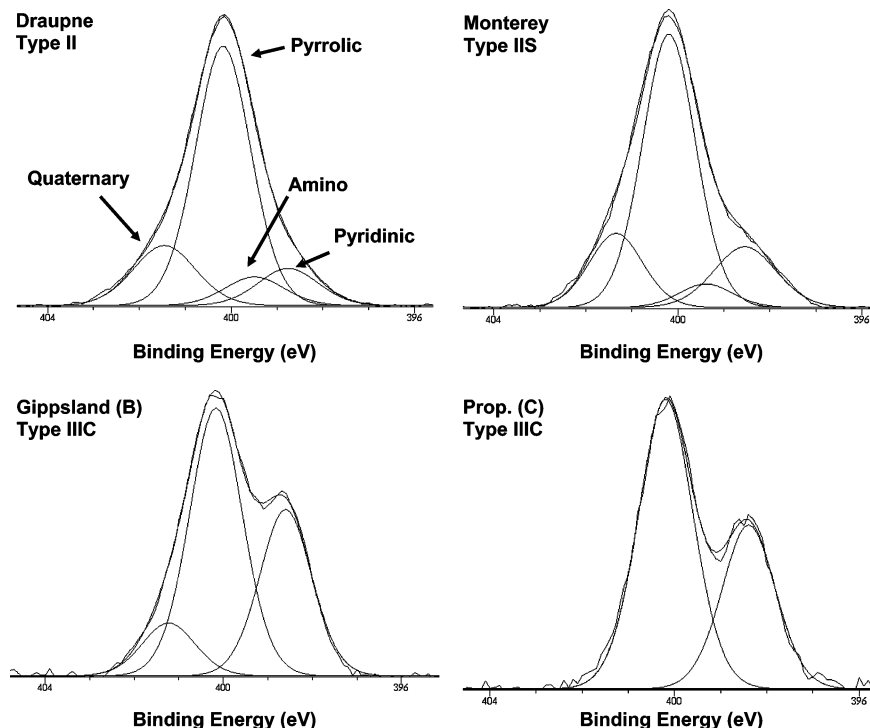


Figure 3. Example XPS nitrogen (1s) spectra for kerogen and curve-resolution into different components.

Table 4. XPS Results for Total Nitrogen and Nitrogen (1s) Curve-Resolution

sample	total per 100 C	mole percent (XPS)			
		pyridinic 398.6 eV	amino 399.4 eV	pyrrolic 400.2 eV	quaternary 401.4 eV
Green River	2.2	20	9	57	13
Rundle	1.8	5	9	52	35
Duvermay (A)	2.9	27	4	52	18
Duvermay (B)	2.0	19	4	59	18
Duvermay (C)	2.1	18	0	65	17
Duvermay (D)	2.1	15	0	62	23
Oxford Clay	2.4	17	15	53	15
Paradox	3.1	23	5	59	13
Malm	2.3	15	9	54	22
Draupne	2.3	10	8	65	17
Bakken	3.5	20	7	52	21
Monterey	3.3	16	5	62	17
Gippsland (A)	0.8	18	0	62	20
Gippsland (B)	1.9	34	0	56	10
Proprietary (A)	1.7	31	0	57	11
Proprietary (B)	1.1	35	0	57	7
Proprietary (C)	1.1	36	0	64	0
Fruitland	1.7	30	0	57	13

↓ = thermal maturity sequence A= immature B-C = oil window, D = post-mature

quality of fits. It also did not affect the relative population of aliphatic and aromatic forms. For this reason only, aliphatic sulfide and thiophenic model compound spectra were used in the curve fitting nonoxidized organic sulfur forms and are reported as aliphatic sulfur and aromatic sulfur to reflect the uncertainty in distinguishing among specific aliphatic and aromatic sulfur forms. The positions attributed to pyrite, sulfate, aliphatic, and aromatic forms are indicated in Figures 9 and 10.

3. Discussion

Characterization of kerogens by solid-state methods offers the opportunity to determine their average chemical composition and structural relationships that may be lost or altered by thermal or chemical degradation methods. The use of multiple techniques that provide complementary information further allows us to evaluate the influences of sample preparation and surface effects that may bias the results.

As expected, the relationship between H/C and O/C ratios delineate kerogens into different types of organic matter. A van

Krevelen diagram was constructed using hydrogen from elemental analysis and organic oxygen from XPS analysis (Figure 11). The fields, defined as types I, II, and III, are based on empirical observations and, although they cannot be used as rigorous guides, are typically associated with lacustrine, marine, and terrigenous (coaly) source environments. As kerogens thermally mature, their O/C and H/C ratios decrease during catagenesis and eventually converge at metagenic levels of maturity. The kerogens used in this work clearly map on a van Krevelen diagram into distinct organic matter type and the types II and IIIC cover a range of maturity spanning the oil window.

Solid-state ^{13}C NMR and XPS are two complementary techniques for determining the amount of aromatic carbon in solid carbonaceous materials. XPS is sensitive to the first 50 Å of the sample while the ^{13}C NMR signals come from the entire sample. There is a good relationship between the hydrogen content and the percent aromatic carbon determined either by XPS or ^{13}C NMR techniques (Figure 12). This agreement implies that the surface composition of finely ground kerogen is close to the bulk average for all kerogens studied.

As one would expect, hydrogen content decreases with an increasing amount of aromatic carbon independent of organic matter type. This trend is followed as a kerogen matures; however, these properties cannot be used as an absolute measure of thermal maturity unless one has knowledge of the initial values of the kerogen prior to the onset of catagenesis. This is illustrated by comparing the Rock-Eval T_{max} , the temperature of maximum pyrolyzate yield at 25 °C/min as measured by the pyrolyzer, with the amount of aromatic carbon. Rock-Eval T_{max} values for types II and IIIC kerogens increase in a linear fashion with increasing thermal maturity; however, the kerogens follow separate trends (Figure 13). There are insufficient data to draw a conclusion concerning the behavior of type I kerogen. For coals, the percent of aromatic carbon similarly increases with increasing vitrinite reflectance, another measure of thermal exposure.²³

Solid-state ^{13}C NMR provides additional details about the structures of carbon present in kerogen. The average number

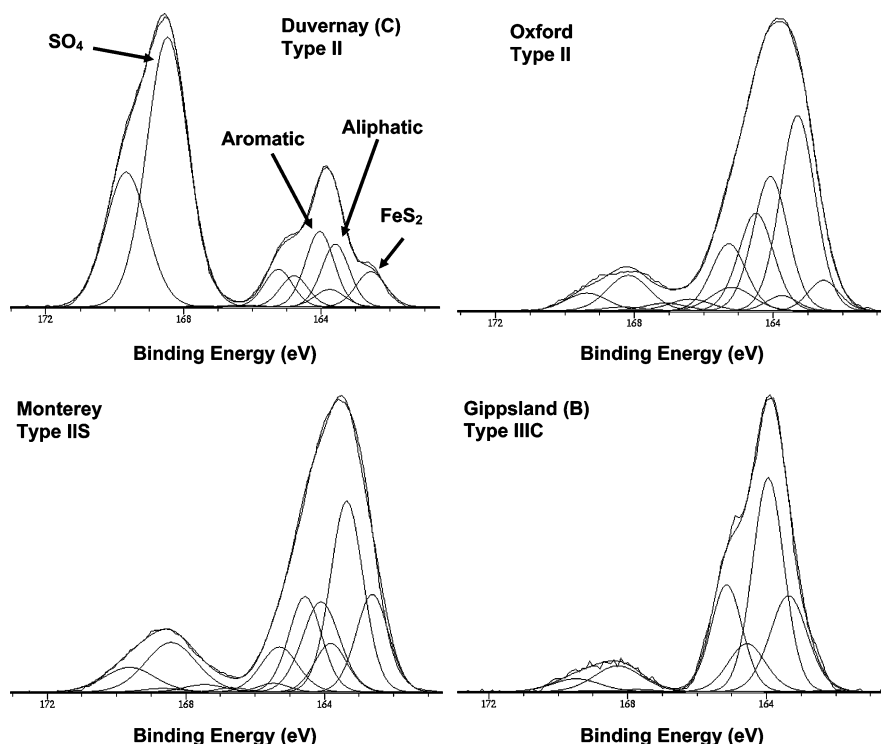


Figure 4. Example XPS sulfur (2p) spectra for kerogen and curve-resolution into different components.

Table 5. XPS Results for Total Organic Sulfur and Sulfur (2p) Curve-Resolution

sample	per 100 carbon	mole percent				
		total org. sulfur	aliphatic sulfur	aromatic sulfur	sulfoxide	sulfate
Green River	0.5	17	10	9	50	14
Rundle	0.6	15	9	4	66	6
Duvernay (A)	1.4	33	28	13	25	2
Duvernay (B)	1.2	16	20	5	46	13
Duvernay (C)	0.6	11	13	0	69	7
Duvernay (D)	1.0	5	20	5	66	4
Oxford Clay	3.2	37	23	10	17	13
Paradox	1.4	16	22	2	45	15
Malm	1.9	22	16	7	45	10
Draupne	2.1	19	20	8	52	1
Bakken	2.2	25	32	10	30	2
Monterey	2.7	39	21	4	16	20
Gippsland (A)	2.7	36	44	8	10	2
Gippsland (B)	0.5	31	58	0	11	0
Proprietary (A)	0.2	24	33	0	42	0
Proprietary (B)	0.2	22	58	0	20	0
Proprietary (C)	0.1	8	56	0	36	0
Fruitland	0.4	37	51	0	12	0

↓ = thermal maturity sequence A= immature B-C = oil window, D = post-mature

Table 6. Definition of Solid-State ^{13}C NMR Structural and Lattice Parameters

structural parameter	chemical shift range (ppm)	carbon type
fa	90–240	aromatic/carboxyl/carbonyl/amide
fa'	90–165	aromatic
fa ^C	165–240	carboxyl/carbonyl/amide
fa ^H	90–135 (–DD)	protonated aromatic
fa ^N	90–165 (DD)	nonprotonated aromatic
fa ^P	150–165	phenoxy/phenolic
fa ^S	135–150	alkyl-substituted aromatic, biaryl
fal	0–90	aliphatic
fal ^H	22–90- (50–60)	methylene/methine
fal*	0–22 & 50–60	methyl/methoxy
fal ^O	50–90	alcohol/ether

lattice parameter	definition	description
FAA	(fa ^P + fa ^S)/fa'	fraction of aromatic carbons with attachments
Cn'	fal/fa ^S	average aliphatic carbon chain length
fa ^B	fa ^N – fa ^P – fa ^S	bridgehead aromatic
C		average carbons per aromatic cluster

of aromatic carbons per cluster (C) is shown in Figure 14. For type II kerogen, C increases from approximately 12, at low aromatic carbon levels, to approximately 20 for the most mature kerogens with high levels of aromatic carbon. For type IIIC kerogen, C also increases with increasing aromatic carbon; however, all data points fall to the right of the type II kerogen samples. The conclusion that the average aromatic carbon cluster size (C) increases with increasing kerogen maturity is further substantiated by the convergence of types II and IIIC data by replacing the ordinate of Figure 14 with Rock-Eval T_{max} . Figure 14 indicates that all kerogens considered in the present study possess on average between 2- to 5-ring aromatic units (12–20 aromatic carbons per cluster) and that the average aromatic carbon ring size increases with increasing kerogen maturation. These structural changes can occur through the selective loss of smaller aromatic ring sizes or by aromatization of adjacent aliphatic carbon structures during kerogen maturation. The aromatic carbon ring sizes for bituminous coal are close to those

observed for type IIIC kerogen at comparable levels of aromatic carbon.¹³ Wei et al.⁵⁵ used similar ^{13}C NMR methods to describe the carbon structure of kerogens from the Tarim Basin, China. These kerogens were isolated from shales Jurassic–Triassic age and are mostly composed of hydrogen-poor coaly macerals that varied in thermal maturity (%R, vitrinite reflectance from 0.52 to 1.81). Results were compared to a dataset from a ^{13}C NMR study of hydrogen-rich type II kerogens from Chinese marine carbonates.⁵⁶ Roughly linear and parallel trends between thermal maturity and aromatic cluster size (fraction of carbon as bridgehead carbon) were reported for the two types of kerogens. The hydrogen-rich kerogens followed a trend very similar to what we observe, but the kerogens from the coaly shales are

(55) Wei, Z.; Gao, X.; Zhang, D.; Da, J. *Energy Fuels* **2005**, *19*, 240–250.

(56) Zeng, F.; Cheng, K. *Earth Sci. Front.* **2000**, *7*, 249–255; in Chinese.

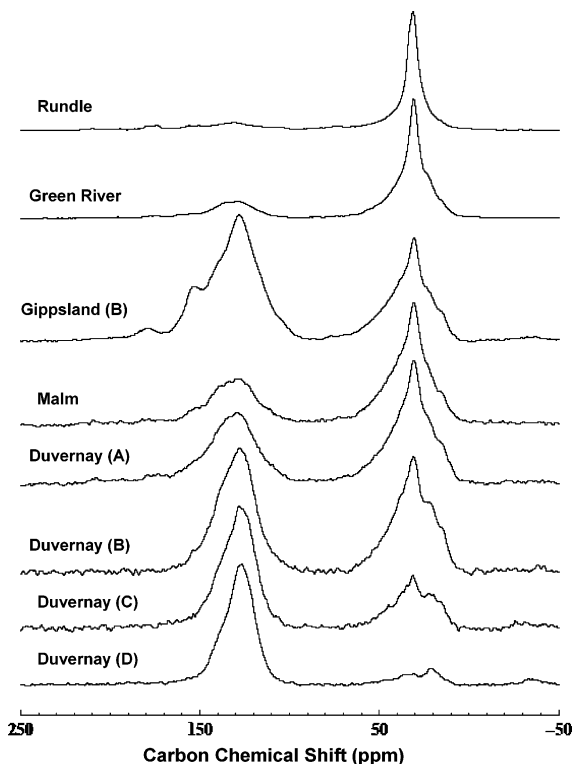


Figure 5. Solid-state ¹³C NMR spectra for kerogen.

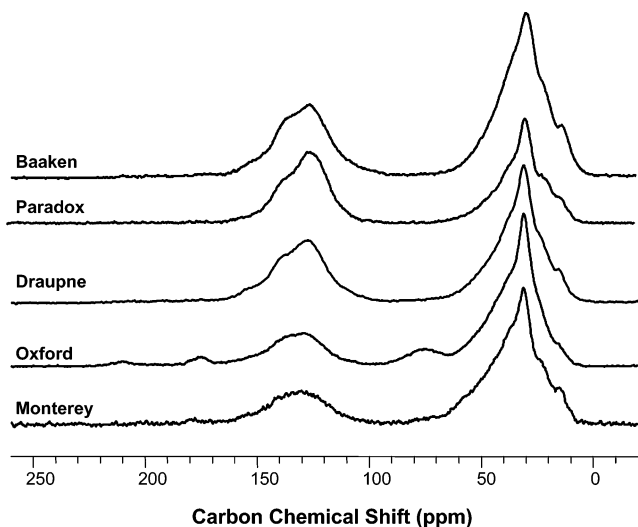


Figure 6. Solid-state ¹³C NMR spectra for type II kerogen.

offset, with aromaticity about 2.5 times that of the carbonate kerogens at equivalent %R values. Wei et al.⁵⁵ suggested that clay minerals catalyzed the thermal reactions associated with kerogen transformation (e.g., loss of heteroatomic functional groups, alkyl chain cleavage, and condensation) such that a higher degree of aromatization is obtained by kerogens in a shale matrix compared to kerogens in a carbonate matrix at equivalent levels of thermal stress. We see no evidence for such mineralogical effects as both our types II and IIIC kerogen maturity suites are from shales and do not exhibit the enhanced degree of aromaticity reported for the Tarim Basin coaly shale kerogens.⁵⁵ In contrast, all of our results agree well with values reported for the hydrogen-rich kerogens. A possible explanation for the high aromaticity of the Tarim Basin samples lies in the origin of the kerogen. Jurassic–Triassic coals and coaly shales in the Tarim Basin are mostly gas-prone. Vitrinite and inertinite constitute most of the structural macerals, with inertinite

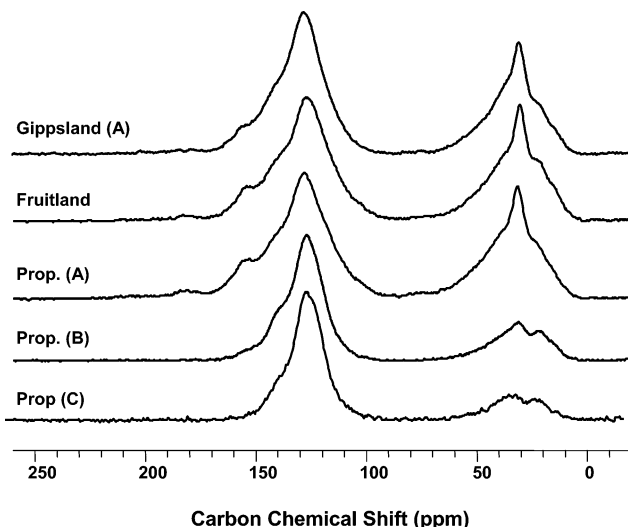


Figure 7. Solid-state ¹³C NMR spectra for type IIIC kerogen.

Table 7. Solid-State ¹³C NMR Structural Parameters for Kerogen

sample	per 1.0 carbons												
	fa	fa ^c	fa ^a	fa ^h	fa ^N	fa ^s	fa ^S	fa ^o	fa ^l	fa ^{l'}	fa ^{l*}	fa ^{l''}	
Green River	0.28	0.03	0.25	0.07	0.18	0.03	0.07	0.08	0.72	0.56	0.16	0.05	
Rundle	0.25	0.06	0.19	0.07	0.12	0.03	0.05	0.04	0.75	0.63	0.12	0.07	
Duvernay (A)	0.46	0.06	0.40	0.13	0.27	0.05	0.12	0.10	0.54	0.39	0.15	0.07	
Duvernay (B)	0.51	0.01	0.50	0.15	0.35	0.03	0.13	0.19	0.49	0.34	0.15	0.04	
Duvernay (C)	0.56	0.02	0.54	0.17	0.37	0.03	0.13	0.21	0.44	0.31	0.13	0.05	
Duvernay (D) ↓	0.82	0.02	0.80	0.28	0.52	0.03	0.16	0.33	0.18	0.11	0.07	0.02	
Oxford Clay	0.26	0.04	0.23	0.09	0.14	0.02	0.07	0.07	0.73	0.53	0.13	0.13	
Paradox	0.48	0.01	0.47	0.17	0.24	0.02	0.09	0.14	0.52	0.38	0.12	0.04	
Malm	0.35	0.05	0.30	0.10	0.20	0.03	0.09	0.08	0.65	0.49	0.16	0.10	
Draupne	0.40	0.02	0.39	0.13	0.21	0.02	0.08	0.11	0.60	0.44	0.13	0.06	
Bakken	0.37	0.02	0.35	0.17	0.18	0.02	0.08	0.09	0.63	0.46	0.15	0.06	
Monterey	0.26	0.01	0.25	0.09	0.14	0.02	0.05	0.06	0.74	0.51	0.18	0.11	
Gippsland (A)	0.66	0.04	0.62	0.20	0.42	0.08	0.15	0.25	0.34	0.20	0.09	0.04	
Gippsland (B)	0.64	0.02	0.62	0.29	0.34	0.04	0.12	0.18	0.36	0.27	0.09	0.04	
Proprietary (A)	0.61	0.04	0.57	0.21	0.37	0.07	0.12	0.19	0.39	0.27	0.10	0.06	
Proprietary (B)	0.73	0.01	0.73	0.26	0.49	0.04	0.17	0.28	0.27	0.17	0.08	0.03	
Proprietary (C) ↓	0.81	0.00	0.81	0.43	0.38	0.02	0.11	0.28	0.19	0.14	0.05	0.01	
Fruitland	0.60	0.03	0.57	0.24	0.31	0.05	0.10	0.15	0.40	0.27	0.11	0.05	

↓ = thermal maturity sequence A= immature B-C = oil window, D = post-mature

Table 8. Solid-State ¹³C NMR Lattice Parameters for Kerogen and Lower Limit Estimate for Organic Oxygen

$$fa^C + 0.5(fa^P + fa^O) \times 100$$

sample	C	FAA	Cn'	fa ^c +0.5(fa ^p +fa ^o) (x100)
Green River	16	0.40	10.3	7.0
Rundle	10	0.42	15.0	11.0
Duvernay (A)	12	0.43	4.5	12.0
Duvernay (B)	19	0.32	3.8	4.5
Duvernay (C)	19	0.30	3.4	6.0
Duvernay (D) ↓	20	0.24	1.1	4.5
Oxford Clay	13	0.40	12.5	11.2
Paradox	17	0.29	6.1	4.1
Malm	13	0.40	7.2	11.5
Draupne	17	0.36	7.6	5.8
Bakken	12	0.27	8.2	5.4
Monterey	12	0.28	15.0	7.5
Gippsland (A)	15	0.37	2.3	10.0
Gippsland (B)	14	0.31	3.1	5.5
Proprietary (A)	16	0.35	3.4	10.2
Proprietary (B)	19	0.26	1.6	3.6
Proprietary (C) ↓	18	0.15	1.8	1.2
Fruitland	14	0.32	3.8	7.9

↓ = thermal maturity sequence A= immature B-C = oil window, D = post-mature

averaging about 33%.⁵⁷ In contrast, the oil-prone type IIIC kerogens in our study are mainly (~90%) composed of

(57) Liu, D.; Tu, J.; Jin, K. *J. Pet. Geol.* 2003, 26, 105–124.

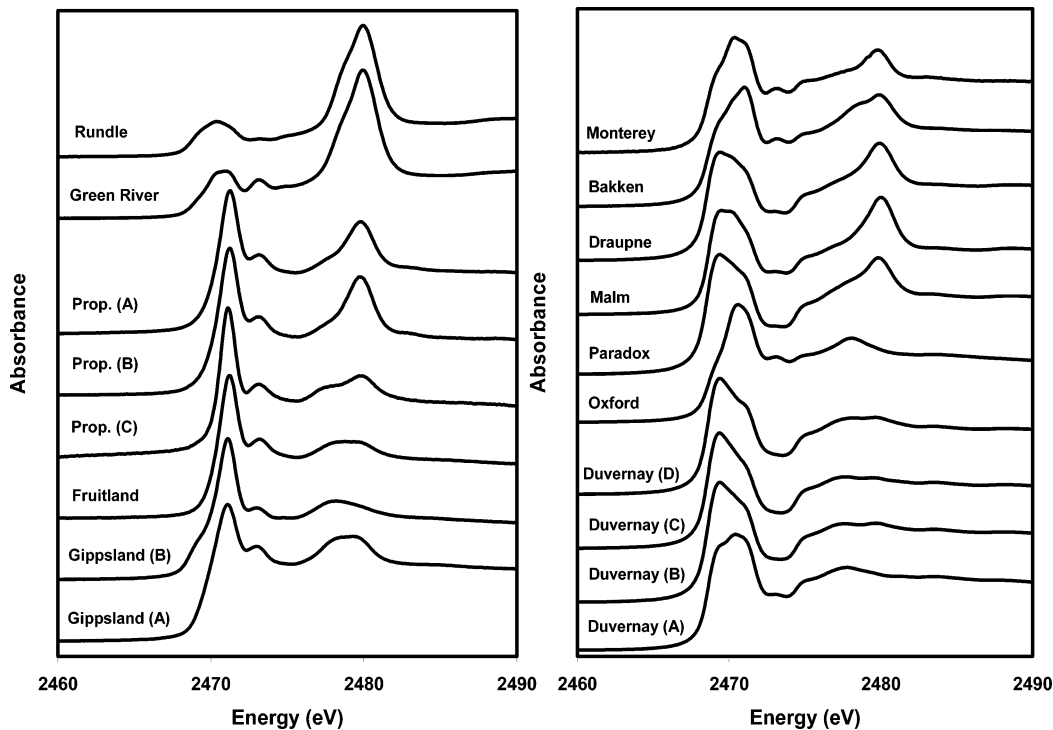


Figure 8. S-XANES absorbance spectra of kerogen.

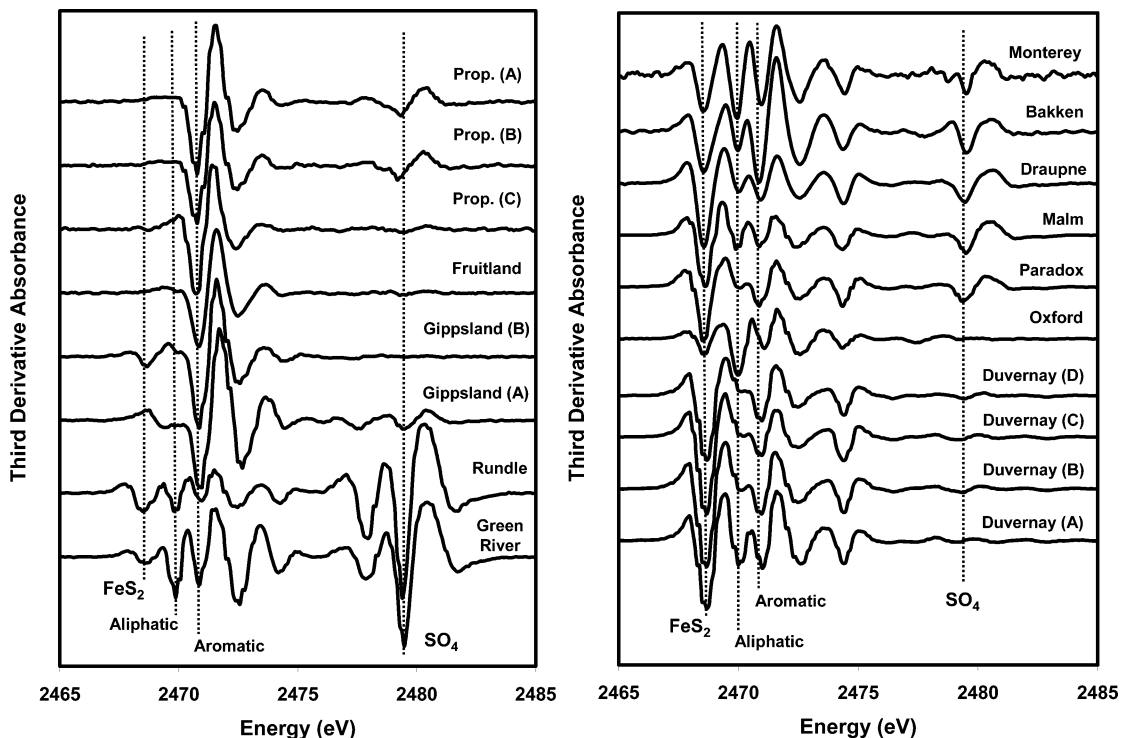


Figure 9. S-XANES third derivative and absorbance spectra of kerogen.

perhydrous vitrinite with minor amounts of exinite. The offset in the aromaticity of the Tarim Basin samples, thus, may be explained not by clay catalysis but by a major contribution of highly aromatic inertinite. This inertinite arose from eroded, overmature sediments that were deposited syngenetically with primary organic matter, which is mostly terrestrial plant debris. Hence, while the reported vitrinite reflectance is measuring the maturity of the primary organic matter, the aromaticity as measured by ^{13}C NMR is an average value reflecting the carbon structure of both the primary organic matter and the reworked inertinite. This conclusion is supported by the very low HI and

OI values reported for these samples⁵⁵ but could be fully substantiated by an optical petrographic analysis.

The average aliphatic carbon chain length (Cn') is determined from the NMR fraction of aliphatic carbon f_a divided by the fraction of aromatic carbon side chains f_a^s . The pattern of Cn' decreasing with increasing amount of aromatic carbon appears to be independent of kerogen organic matter type (Figure 15). Remarkably, this relationship is virtually identical to the one found for coal, peat, and pyrolyzed peat.²³ Cn' approaches a value of 1.0 for kerogens and coals with the highest levels of aromatic carbon. This indicates that almost all aliphatic carbon

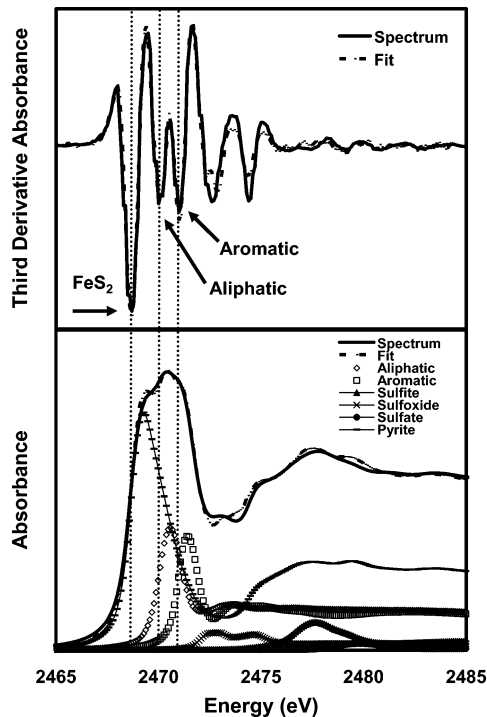


Figure 10. S-XANES absorbance and third derivative absorbance edge spectra of Duvernay (A) kerogen and the results of curve fits using spectra from model compounds.

Table 9. Results of Fits to the S-XANES Third Derivative Spectrum

sample	mole percent				
	aliphatic sulfide	aromatic (thiophenic)	sulfoxide/sulfone	SO ₃ /SO ₄	pyrite
Green River	20	16	8	49	6
Rundle	8	6	7	71	8
Duvernay (A)	22	21	4	1	52
Duvernay (B)	10	16	3	1	70
Duvernay (C)	8	12	2	1	77
Duvernay (D)	7	15	3	4	71
Oxford Clay	39	22	3	14	22
Paradox	10	16	4	9	61
Malm	15	13	4	10	57
Draupne	11	15	4	9	61
Bakken	21	32	4	16	28
Monterey	33	25	3	10	29
Gippsland (A)	31	31	5	18	15
Gippsland (B)	33	48	3	6	10
Proprietary (A)	43	42	6	9	0
Proprietary (B)	25	59	5	10	0
Proprietary (C)	11	79	2	1	7
Fruitland	31	58	4	6	0

↓ = thermal maturity sequence A= immature B-C = oil window, D = post-mature

exists as methyl groups for kerogens that have passed through the oil window.

The fraction of aromatic carbons with attachments (FAA) decreases with increasing amount of aromatic carbon for types II and III C kerogen maturity sequences (Figure 16). For these kerogens, FAA is roughly 0.4 at the lowest levels of aromatic carbon and declines to about 0.2 at the highest levels of aromatic carbon corresponding to the most mature kerogens in the sequences. For peats, lignites, and higher rank coals, the maximum FAA of 0.4 appears near 40% aromatic carbon.²³ This pattern is observed with kerogen as well. Low aromatic carbon type I kerogens (<30%) have FAA values near 0.4. The FAA values of low aromatic (<50%) type II kerogens varies between 0.28 and 0.42. The FAA results indicate that aromatic carbon is highly substituted in kerogens that have not passed through the oil window.

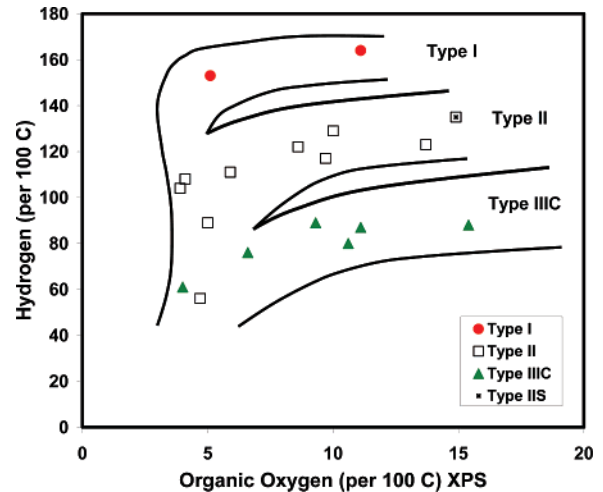


Figure 11. Van Krevelen diagram for kerogen using hydrogen from elemental analysis and organic oxygen from XPS analysis.

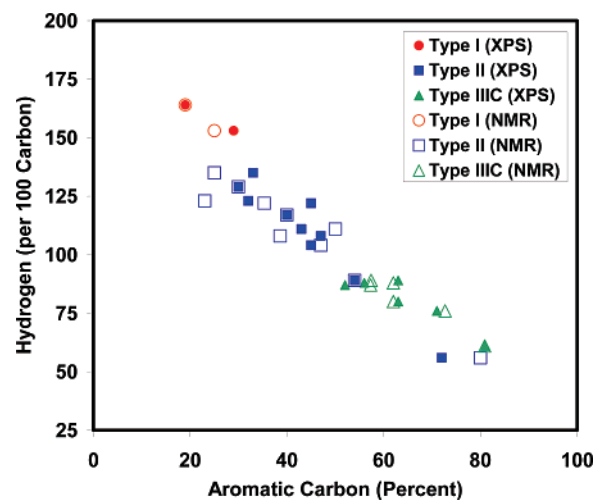


Figure 12. Plot of the amount of hydrogen and the percent aromatic carbon from ¹³C NMR and XPS.

Table 10. Results of Fits to the S-XANES K-Edge Spectrum

sample	mole percent				
	aliphatic sulfide	aromatic (thiophenic)	sulfoxide/sulfone	sulfite and sulfate	pyrite
Green River	21	17	5	50	8
Rundle	17	11	0	57	15
Duvernay (A)	29	24	3	3	41
Duvernay (B)	20	19	3	5	53
Duvernay (C)	15	16	7	1	61
Duvernay (D)	11	21	6	3	60
Oxford Clay	44	26	2	7	22
Paradox	16	18	2	14	49
Malm	26	18	0	19	37
Draupne	21	17	2	17	44
Bakken	24	28	6	11	31
Monterey	33	23	3	11	31
Gippsland (A)	27	43	10	14	5
Gippsland (B)	27	53	1	8	12
Proprietary (A)	28	51	3	16	2
Proprietary (B)	19	62	1	18	0
Proprietary (C)	13	71	2	12	2
Fruitland	19	65	5	11	0

↓ = thermal maturity sequence A= immature B-C = oil window, D = post-mature

There is considerable variation in the total organic oxygen level among the kerogen samples (Figure 11). This is related to the organic matter type and level of maturity. For coal, the main chemical pathways of carbon and oxygen transformations during coalification are generally understood. The total organic oxygen level decreases during coalification. Lignitification of

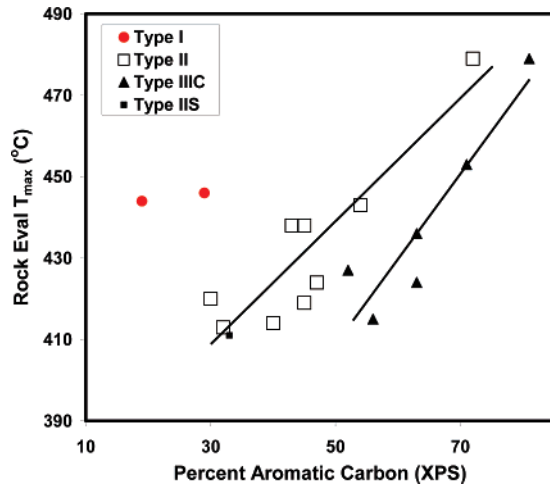


Figure 13. Plot of Rock-Eval T_{max} versus the percent aromatic carbon from XPS.

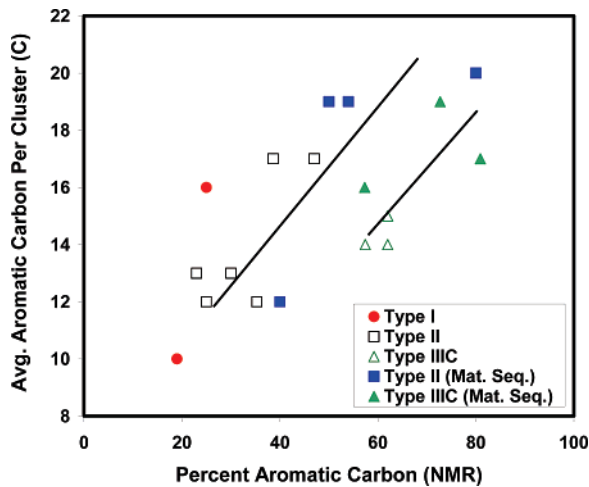


Figure 14. Plot of the average number of aromatic carbons per cluster versus the percent aromatic carbon in kerogen.

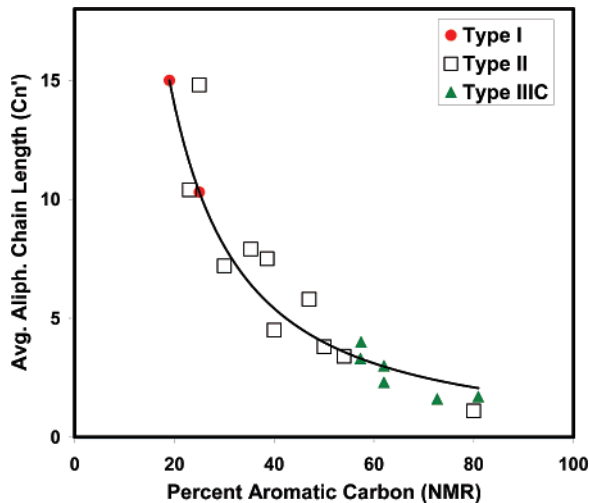


Figure 15. Plot of the average aliphatic carbon chain length and the percent aromatic carbon in kerogen.

peat involves air oxidation followed by decarboxylation and dehydration.⁵⁸ Bituminization of lignite involves decarboxylation and hydrogen disproportionation.⁵⁸ Similar features appear as kerogen matures and the level of aromatic carbon increases.

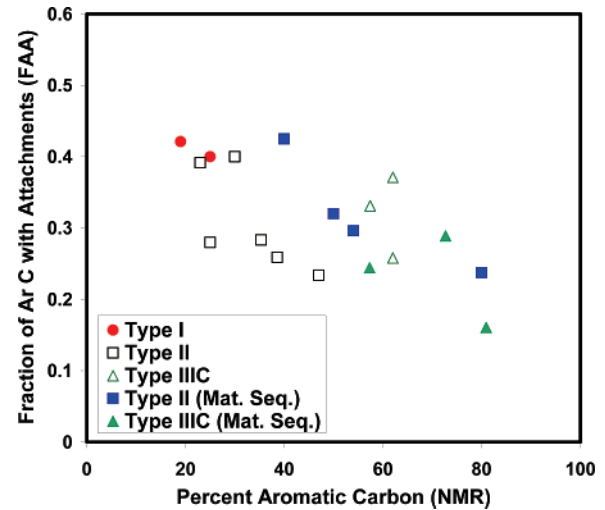


Figure 16. Plot of the fraction of aromatic carbon with attachments and the percent aromatic carbon in kerogen.

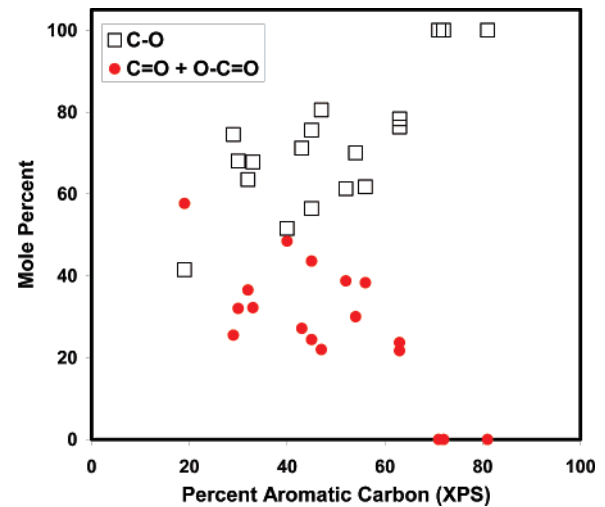


Figure 17. Mole percent carbon oxygen single bond species (C—O) and carbon oxygen multiply bonded species (C=O plus O—C=O) plotted versus the percent aromatic carbon in kerogen.

XPS results show that, on a relative basis, the number of carbon oxygen single bonded species (C—O) increases, while the amount of carbonyl/carboxyl species (C=O plus O—C=O) decreases with an increasing amount of aromatic carbon (Figure 17). This tendency appears independent of the total organic oxygen level and is thus independent of organic matter type.

Solid-state ^{13}C NMR parameters fa^C (carboxyl, carbonyl, amide), fa^P (phenolic, phenoxy), and fa^O (alcohol, ether) have organic oxygen or other heteroatoms associated with them. It is not possible to determine the total amount of organic oxygen relative to carbon from the sum of oxygen related ^{13}C NMR signals (fa^C , fa^P , fa^O) because of the uncertainty in assigning the correct stoichiometry of each oxygen-related ^{13}C NMR signal. Nevertheless, a lower limit estimate for the amount of oxygen associated with fa^C is 1.0 (i.e., ketone, amide, etc.) and 0.5 for fa^P and fa^O (i.e., aliphatic ether, methoxy, etc.). Figure 18 shows a solid-state ^{13}C NMR-derived parameter for organic oxygen, $fa^C + 0.5 \times (fa^P + fa^O)$, plotted versus total organic oxygen as determined by XPS. Some of the measurements fall below the parity line, in agreement with the view that the NMR-derived equation used to estimate the amount of organic oxygen is a lower limit estimate and suggests that hydroxyl species make up a portion of the organic oxygen single bonded species and carboxyl groups contribute to fa^C .

(58) van Krevelen, D. W. *Coal*; Amsterdam: Elsevier, 1993.

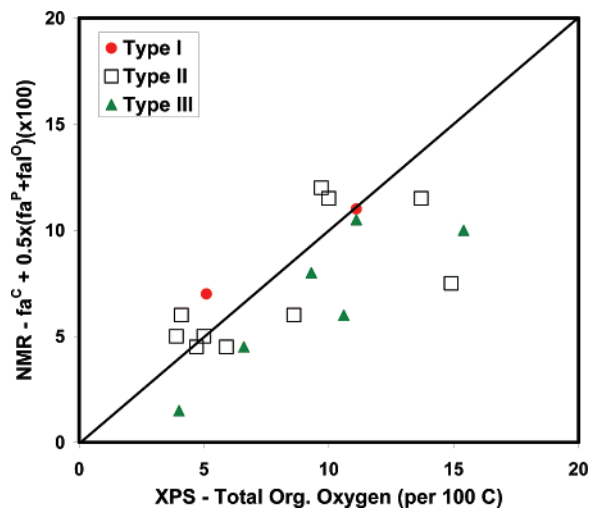


Figure 18. Solid-state ^{13}C NMR derived parameter for organic oxygen $\text{fa}^{\text{C}} + 0.5 \times (\text{fa}^{\text{P}} + \text{fa}^{\text{O}})$ plotted versus total organic oxygen determined from XPS.

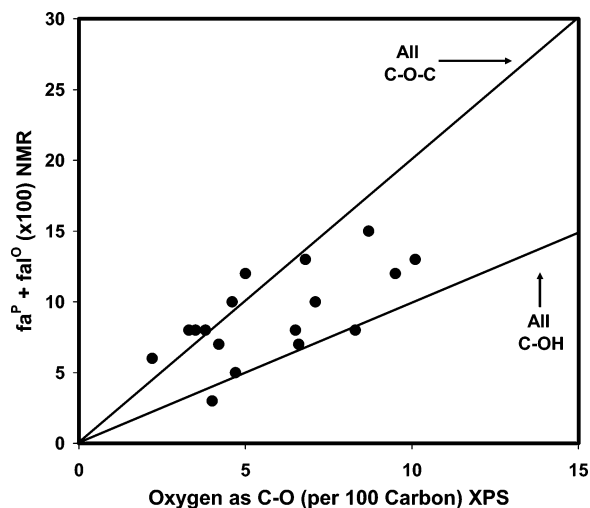


Figure 19. Comparison of solid-state ^{13}C NMR carbon bound to oxygen by single bonds ($\text{fa}^{\text{P}} + \text{fa}^{\text{O}} \times 100$) and oxygen as carbon oxygen single bond species from XPS.

The minimum amount of oxygen associated with fa^{P} and fa^{O} is 0.5 (i.e., ether), and the maximum amount is 1.0 (i.e., alcohol, phenolic, etc.). Figure 19 is a plot of the solid-state ^{13}C NMR number of carbon bound to oxygen by single bonds ($\text{fa}^{\text{P}} + \text{fa}^{\text{O}} \times 100$) versus the XPS derived amount of oxygen associated with carbon oxygen single bond species from XPS. Trend lines indicate the relationships expected for carbon oxygen single bonded species either as all ether or all hydroxyl forms. The comparison of the XPS amount of oxygen associated with functional groups containing carbon oxygen single bonds and ^{13}C NMR results yield self-consistent results that mostly fall between the two limiting situations of exclusive ether or hydroxyl carbon–oxygen bonds.

Total nitrogen varies considerably in the studied samples. Type III kerogens have the lowest proportion of organic nitrogen, while the amount varies widely among the type II kerogens and appears to be highly dependent on organic facies. Figure 20 shows the quantification of organic nitrogen species by XPS plotted versus the amount of aromatic carbon. Pyridinic and quaternary forms have been grouped. It is remarkable that despite large differences in the total organic nitrogen, source of organic matter, and maturity among kerogens, the relative

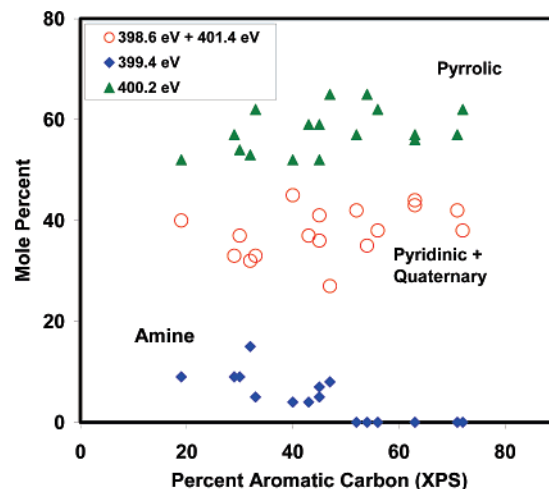


Figure 20. Quantification of organic nitrogen species by XPS.

abundances of pyrrolic and pyridinic nitrogen are comparable and account for the vast majority of nitrogen forms.

Pyrrolic structures represent the most abundant nitrogen form, followed by pyridinic and protonated basic nitrogen structures. Most nitrogen contributed to sediments is derived from proteinaceous amides with secondary amounts of pyrrolic and pyridinic nitrogen derived from other biomolecules, such as nucleic acids and porphyrins. Microbial and thermal decomposition processes may transform the proteinaceous nitrogen into heterocyclic structures that become incorporated into kerogen and coal. These major alterations hamper analytical attempts to trace nitrogen in kerogens and coals back to their biological origins.³⁷

Amides are not thought to be present in abundance in kerogen after early diagenesis. If amides are present in source rock kerogen, they are expected to be hydrolyzed to carboxylic acids and amines during acid demineralization. The amines, in turn, may deaminate. A peak at 399.4 eV is needed to resolve fully the nitrogen (1s) spectrum for the least mature kerogens. This position is consistent with basic amine nitrogen forms. The fact that these amines and pyridinic nitrogen survive demineralization indicates that these species are either in hindered structures or not sufficiently basic to react. The amine peak is not needed to fully curve-resolve the nitrogen (1s) spectrum of high maturity kerogens. Nitrogen XANES analysis of Green River kerogen and bitumen reveal that amine nitrogen is present in low amounts (<15 mol %) relative to the more abundant pyrrolic and pyridinic nitrogen forms.⁴¹ Pyrolysis studies of Green River and Bakken kerogens indicate that that amine nitrogen concentrates in the pyrolysis tar, not in the residue³⁹ suggesting that the amine nitrogen present in immature kerogens is selectively lost during thermal maturation and, therefore, does not appear in more mature kerogens. Recent studies indicate that amide nitrogen is the dominant nitrogen form in unaltered peat but these amide structures are converted/cyclized into pyridinic and pyrrolic nitrogen forms after a thermal stress roughly equivalent to lignitification.²⁶ Again, it is remarkable that the relative abundances of pyrrolic and pyridinic/protonated-basic nitrogen are comparable and account for the vast majority of nitrogen forms regardless of the large differences in total organic nitrogen, source of organic matter, and maturity among the studied kerogens.

Organic sulfur in kerogens may be derived directly from sulfur-containing biomolecules or, more likely, from hydrogen sulfide incorporated during early diagenesis. Most of this sulfide is produced by bacterial sulfate reduction. Consequently,

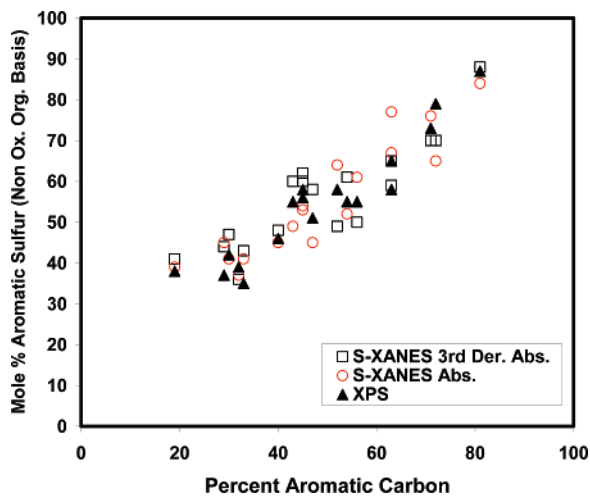


Figure 21. Plot of the mole percent of organic sulfur forms versus percent aromatic carbon from XPS and S-XANES analysis on a nonoxidized organic sulfur basis.

lacustrine systems with no source of sulfate yield kerogens that are relatively depleted in sulfur, while marine environments yield kerogens with varying amounts of organic sulfur depending on the degree and persistence of euxinic conditions and mineralogy. High-sulfur marine kerogens behave quite differently with respect to oil generation kinetics and product yields and are assigned their own designation, type IIS, to distinguish these characteristics from lower sulfur type II kerogens. In reality, there is a continuum with no clear demarcation. Coals and coaly shales may be deposited in continental or near-shore marine environments, yielding kerogens that may vary in organic sulfur content within the same stratigraphic unit. The two Gippsland type IIIC kerogens, containing 2.7 and 0.5 sulfur per 100 carbons, respectively, reflect these different depositional settings.

Organic sulfur forms determined by XPS and S-XANES can be compared on a relative basis. Figure 21 is a plot of the mole percent of organic sulfur forms from XPS, S-XANES third derivative absorbance, and S-XANES absorbance plotted versus percent aromatic carbon on a nonoxidized organic sulfur mole percent basis. These data agree and show that the relative level of aromatic sulfur increases with an increasing amount of aromatic carbon. There is a corresponding decline in aliphatic sulfur forms with an increasing amount of aromatic carbon. In fact, the ratio of aliphatic to aromatic sulfur is proportional to aromatic carbon regardless of kerogen type (Figure 22). A recent K-edge S-XANES study reported that type I kerogens contain higher ratios of aliphatic to aromatic (thiophenic) sulfur than type II kerogens; however, no information was provided concerning the relative maturity of these samples.³⁰

The behavior of organic sulfur in kerogen with increasing maturation appears to be very similar to that in coal.²⁹ The overall pattern for sulfur forms in unaltered peats, lignites, and higher ranked coals shows a progressive increase in the relative abundance of aromatic sulfur forms as coalification progresses from peats.²⁶ S-XANES results also show that aliphatic sulfide, sulfites, mercaptan, and disulfide species are present in unaltered peats.²⁶ These are likely associated with sulfur forms incorporated into the sedimentary matter that are resistant to degradation and survive past early diagenesis. Upon conversion to lignite, sulfite groups are eliminated while mercaptan, disulfide, and aliphatic sulfur species decrease at the expense of increasing aromatic sulfur.²⁶ Mercaptan and disulfides are not found in higher rank coals where aliphatic sulfide is the predominant form.²⁹ It is likely that mercaptans condense to form sulfides, liberating H₂S, and that disulfides decompose to form sulfides.

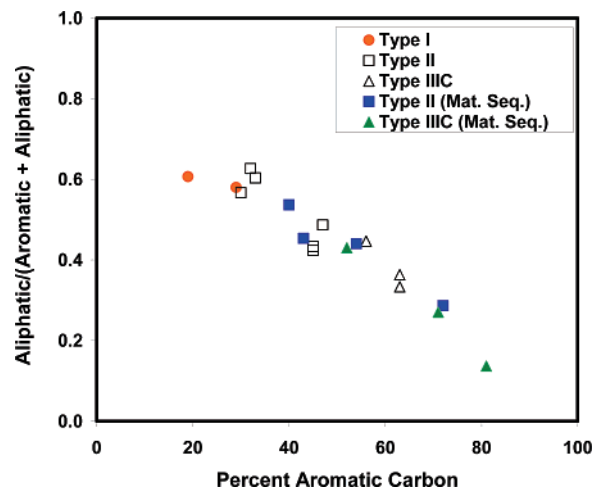


Figure 22. Comparison of the ratio of aliphatic to aliphatic plus aromatic sulfur to percent aromatic carbon. Organic sulfur measurements are averaged from XPS and S-XANES analyses.

S-XANES and XPS results show that small amounts (<10 mol %) of sulfoxides are present in most kerogens. Small amounts of sulfoxides have been observed in other S-XANES analyses of kerogen.^{30,32} Sulfoxides do not appear in carefully sampled and preserved coals^{28,29} suggesting that the sulfoxides seen in the kerogens are due to sample oxidation. However, the origin of the sulfoxides in kerogen, whether naturally occurring or introduced during sample preparation, has not been addressed.^{30,32} Nonaromatic sulfur forms in coal appear more prone to ambient oxidation.⁵⁹ If the sulfoxides in kerogen have a similar origin, then these species would increase slightly the relative amounts of aliphatic sulfur forms.

The presence of significant amounts of pyrite and iron sulfate is confirmed in types I and II kerogen samples. FeS₂ and sulfate sulfur signals are evident in the curve-resolved XPS 2p spectrum. Corresponding iron signals appear, respectively, at 707 and 711 eV. It is likely that iron sulfate is a surface oxidation product of pyrite. Pyrite is differentiated from elemental sulfur forms in S-XANES by its appearance at 0.5 eV lower energy in the third derivative of the absorbance spectrum. The presence of pyrite is not easily spotted in the absorbance spectrum as it is in the third derivative of the spectrum. It is possible that even in the third derivative of the spectrum that relatively high amounts of pyrite can obscure detecting the presence of lesser amounts of disulfides and elemental sulfur. Wiltfong et al.³⁰ showed that curve fits to the low energy portion of the sulfur K-edge XANES absorption spectra of types I and II kerogens were slightly better using elemental sulfur than using pyrite as a fitting component; however, the resolution is not sufficient for a definitive assignment. The appearance of sulfate together with pyrite in our kerogen samples suggests that oxidation of pyrite may have occurred and that elemental sulfur could be another product associated with this oxidation.

XPS and S-XANES results clearly show that the ratio of aliphatic to total organic sulfur decreases as the level of aromatic carbon increases with sample maturity regardless of kerogen type. Unlike peat and lignite, disulfide sulfur species were not needed to obtain good fits to the S-XANES third derivative of the absorbance spectrum. This may in part be due to the presence of significant quantities of pyrite that would obscure the resolution of disulfide species at low abundances. However,

(59) Gorbaty, M. L.; Kelemen, S. R.; George, G. N.; Kwiatek, P. J. *Fuel* 1992, 71, 1255.

slightly better objective fits were obtained when disulfides were included in the curve-resolution procedure of the least mature kerogen samples (e.g., Monterey, Oxford Clay, and Gippsland (A)). For self-consistency, these results are not reported, but disulfides never exceeded $1/3$ of total aliphatic sulfur pool for these kerogens. Disulfides are identified by L- and K-edge XANES in thermally immature sulfur-rich kerogens that were free of pyrite.^{32,33} Alkyl sulfides and thiophenic sulfur also were identified in these kerogens.^{32,33}

By tracing carbon and heteroatom speciation in different types of kerogens, the underlying structural properties that give rise to these classifications are revealed. Furthermore, changes in abundance and speciation of organic nitrogen and sulfur can be traced as a function of thermal maturation, much like van Krevelen showed for hydrogen- and oxygen-to-carbon ratios. The enhanced information provided by direct chemical characterization offers additional details about the organic species within kerogens that can provide a basis for developing both specific and general average chemical structural models. These structural representations can be coupled with known reaction pathways to predict their thermal conversion to products upon heating under laboratory (i.e., degrees Celcius per minute) or geologic (i.e., degrees Celcius per million years) conditions. For example, a prior study used carbon structural and lattice parameters derived from solid-state ^{13}C NMR analysis to develop chemical structural descriptions of coal and these structures were coupled to reactivity models (chemical percolation devolatilization) to predict tar and char yields during coal pyrolysis.⁹ The models in this study did not include nitrogen and sulfur heteroatom structures as only elemental data was available and the internal distribution of these heteroatoms was unknown. Using the knowledge provided by solid-state analyses, it is possible to develop more comprehensive approaches for inclusion of nitrogen, sulfur, and oxygen heteroatoms into kerogen chemical structure models.^{43,44} The correct distributions of heteroatomic structures are important for predicting reactivity and physical properties. For example, the cleavage of weak aliphatic sulfur bonds promotes early petroleum generation

(60) Kelemen, S. R.; Walters, C. C.; Ertas, D.; Kwiatek, L. M.; Curry, D. J. *Energy Fuels* **2006**, *20*, 301.

(61) Kelemen, S. R.; Walters, C. C.; Ertas, D.; Freund, H. L. M.; Curry, D. J. *Energy Fuels* **2006**, *20*, 309.

during the maturation of high-sulfur kerogens. Heteroatom structures also affect the solubility parameter and cross-link density of kerogen that influences the mechanism involved in the expulsion of petroleum from kerogen.^{60,61}

Summary

Kerogens spanning a range of organic matter types and thermal maturation were characterized using a combination of solid-state X-ray and ^{13}C NMR methods. Carbon structural and lattice parameters indicated that the percent aromatic carbon increases with increasing thermal maturity for hydrogen-rich types II and III kerogens, but these organic matter types follow different trends. With increasing amounts of aromatic carbon, the fraction of aromatic carbons with attachments (FAA) generally decreases and the average aliphatic carbon chain length (Cn') decreases, while the average number of aromatic carbons per cluster (C) increases. FAA values range from 0.2 to 0.4, and C values range from 12 to 20 indicating that kerogen possesses on average 2- to 5-ring aromatic carbon units that are highly substituted. XPS and ^{13}C NMR results agree on the forms and the amount of organically bound oxygen. Carbonyl-carboxyl species decrease with an increasing amount of aromatic carbon while carbon oxygen single bonded species increase. XPS analyses indicate that the majority of nitrogen exists as pyrrolic nitrogen, and the relative abundance of pyrrolic nitrogen is comparable in all kerogens and maturity levels. S-XANES and XPS results show that the relative level of aromatic sulfur increases with an increasing amount of aromatic carbon for all kerogens. These generalizations for relative abundances of nitrogen and sulfur species appear to hold in spite of large differences among kerogens in the total amounts of organic nitrogen and sulfur.

Acknowledgment. Use of the Advanced Photon Source was supported by the U.S. Department of Energy, Basic Energy Sciences, Office of Science, under contract no. W-31-109-Eng-38. We are grateful for the help and support received from Ms. T. Bolin and Dr. T. Gog at the Advanced Photon Source at Argonne National Laboratory. We thank Mr. B. Liang for conducting the NMR experiments and Dr. J. W. Larsen for CrCl_2 treatment of Monterey kerogen.

EF060321H